

Directly detecting sub-MeV dark matter via 3-body inelastic scattering process

Wei Chao,^{*} Mingjie Jin[†], and Ying-Quan Peng[‡]

Center for Advanced Quantum Studies, Department of Physics, Beijing Normal University, Beijing, 100875, China



(Received 11 October 2021; accepted 11 May 2023; published 30 May 2023)

Direct detection of sub-GeV dark matter (DM) is challenging because the recoil energy of the nuclei or electron from the elastic scattering of a sub-GeV DM off the target can hardly reach the detector threshold. In this paper, we present a new direct detection strategy for sub-MeV DM via the three-body inelastic scattering process, $DM + DM + T \rightarrow \eta + T$, where η is either a DM composite state or any dark radiation, T is the detector target. This process is common for a large class of DM models without presuming particular thermal history in the early Universe. The typical signature from this process is almost a monoenergetic pulse signal where the recoil energy comes from either the binding energy or the consumed DM particle. We show that detectable DM mass range can be effectively enlarged compared to the elastic scattering process.

DOI: [10.1103/PhysRevD.107.093009](https://doi.org/10.1103/PhysRevD.107.093009)

I. INTRODUCTION

Despite ample evidence of dark matter (DM) in our Universe, its particle nature (mass, spin, and coupling) is still a mystery. The unknown mass of possible DM, ranging from 10^{-22} eV to 10^{55} GeV, leaves the experimental observation of DM a severe challenge. Many ideas have been proposed to search for DM in laboratory [1,2]. Assuming DM origins from thermal processes in the primordial plasma, its mass range is limited to [$\mathcal{O}(1)$ keV, $\mathcal{O}(100)$ TeV], where the upper bound is required by the unitarity constraint on DM annihilation amplitude [3] and the lower bound is required by the large scale structure of the Universe [4]. This kind of DM can be directly detected in underground laboratory by looking for kinetic energy deposited by DM scattering on atomic nuclei. The direct detections for DM have reached great sensitivities and give the current most stringent limits for DM masses above a few GeV [5–8]. However, the traditional direct detection of DM via $2 \rightarrow 2$ elastic scattering process loses sensitivity rapidly for a sub-GeV DM because the recoil energy turns out to be smaller than the detector threshold.

Many new approaches have been proposed for the direct detection of sub-GeV DM, for example, boosted DM via various cosmic rays [9–13]; inelastic DM scattering off target nuclei, during which additional excitations are created [14–26]; the absorption of a fermion DM by target and emit a nearly massless neutrino [27–29], which produces a characteristic signal; searching DM using condensed matter system [30–36], where excitations in condensed matter systems provide promising signals; large energy transfer induced by deexcitation of targets [37,38]; considering the Migdal effect [39–44], which results in an inelastically excited electron; detecting DM in superconductors [45], which stand out with the lowest threshold, etcetera. So far, these approaches may reach to a very low mass regime, but some of them are only applicable to specific DM models. A new strategy is still needed to detect the lower mass regime.

In this paper, we propose a new direct detection strategy for sub-MeV DM via the three-body inelastic scattering process, $DM + DM + T \rightarrow \eta + T$, where T is the target and η is either a DM composite state or any dark radiation. If η is a bound state of DM, then its binding energy and kinetic energy can be transferred to the target during the scattering, which results in enhanced recoil energy. Alternatively, if η is a dark radiation, then two DM masses are consumed during the scattering, which significantly improve the recoil energy. Notice that the Co-SIMP [46] scenario also adopts $3 \rightarrow 2$ for direct detection, but our proposal is essentially different from theirs since it is based on renormalizable DM interactions and does not depend on the specific thermal history of DM. We find that there might still exist sizable $3 \rightarrow 2$ process in direct

^{*}chaowei@bnu.edu.cn

[†]jinnmj507@gmail.com

[‡]yqpenghep@mail.bnu.edu.cn

Published by the American Physical Society under the terms of the Creative Commons Attribution 4.0 International license. Further distribution of this work must maintain attribution to the author(s) and the published article's title, journal citation, and DOI. Funded by SCOAP³.

detections for DM models where their relic abundance arises solely from $2 \rightarrow 2$ annihilation. In addition, the $3 \rightarrow 2$ inelastic scattering naturally exists in composite DM model. Although the $3 \rightarrow 2$ scattering cross section is small, the high DM density as well as the high SM target density make this process detectable.

In the following, we first describe the setup and main features of $3 \rightarrow 2$ process. Then we present two specific DM models and study constraints of 3-body DM-electron scatterings. Following that, the effect induced by the 3-body DM-nuclei scattering is also discussed. Finally we summarize our main conclusion. Details of our calculation are given in the Appendices.

II. $3 \rightarrow 2$ PROCESSES IN DM DIRECT DETECTIONS

Previous studies of DM direct detection mainly focus on $2 \rightarrow 2$ process which is either elastic or inelastic. In this section, we consider the signal of the $3 \rightarrow 2$ DM-target scattering process. The $3 \rightarrow 2$ process has been widely applied to address the spectroscopy and relic density of the strongly interacting massive particles (SIMPs) [46–53], but a similar process is not studied with dedication in DM direct detections. Compared with the $2 \rightarrow 2$ process, the target receives more recoil energy in the $3 \rightarrow 2$ process. Thus this process is more suitable for the direct detection of light DM. In general, the maximum recoil energy in $2 \rightarrow 2$ elastic scattering process is $E_R^{\max} = 2\mu^2 v^2 / m_N$ and $E_R^{\max} \approx \frac{1}{2} m_{\text{DM}} v^2$ for nucleus and electron, where m_{DM}, m_N denote the mass of DM and nucleus, respectively, μ is the reduced mass of the DM and nucleus, and $v \approx 10^{-3}$ is the initial velocity of DM. In the $3 \rightarrow 2$ process, the transferred energy to the target particle is $\Delta E = (4 - \xi^2) m_{\text{DM}}^2 / (2m_T + 4m_{\text{DM}})$, where we have neglected the initial kinetic energy of DM, and $\xi \equiv m_f / m_{\text{DM}}$ denoting the mass ratio of final and initial dark sectors, and m_T is the target mass. As a result, the recoil energy for electron is $E_R = \Delta E - |E_B|$, where E_B is the binding energy of electron, while $E_R = \Delta E$ for nucleus.

For the case of the xenon target, we consider 11 different binding energy of the electron in xenon shell (n, l), thus the naive recoil energy without ionization form factor for electron is determined by $E_{R,i} = E_R^{\max} - |E_{B,i}|$ ($i = 1s^2, \dots, 5p^6$), where corresponding binding energies are given in Ref. [54]. We show in Fig. 1 the typical recoil energy E_R as a function of m_{DM} in $2 \rightarrow 2$ and $3 \rightarrow 2$ scattering processes, respectively. It shows that the required DM mass in the $3 \rightarrow 2$ inelastic scattering is much smaller than that in the $2 \rightarrow 2$ elastic process at same recoil energy.

For the $3 \rightarrow 2$ process, the event rate per unit time per unit energy per unit detector mass for a target to recoil with energy E_R can be written as

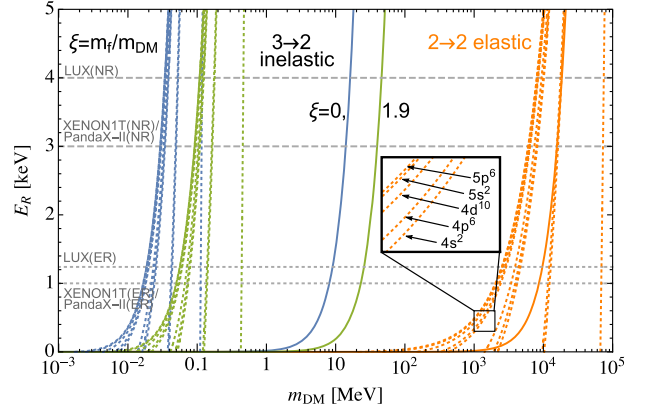


FIG. 1. The recoil energy E_R versus m_{DM} in the $2 \rightarrow 2$ elastic and the $3 \rightarrow 2$ inelastic scattering processes. The orange solid line denotes recoil energy of nucleus from the $2 \rightarrow 2$ process, and the blue, green lines describe recoil energy of nucleus from the $3 \rightarrow 2$ process with $\xi = 0, 1.9$, respectively. Same color labels but instead dotted lines describe the electron recoil energy from the $2 \rightarrow 2$ and $3 \rightarrow 2$ processes. There are 11 different binding energy of electrons in xenon shell and a fraction of xenon electron shells are shown in the inset. As a comparison, the horizontal gray dashed and dotted lines represent the nuclear recoil (NR) and electron recoil (ER) threshold of current xenon-based experiments [55–60], respectively. For binding energy for xenon electron shells, see Table I for detail.

$$\frac{dR_{3 \rightarrow 2}}{dE_R} = N_T \int d^3 v_1 d^3 v_2 n_{\text{DM}}^2 v_1 v_2 \frac{d\sigma_{3 \rightarrow 2}}{dE_R}, \quad (1)$$

where N_T is the number of target per unit detector mass, n_{DM} is the DM density, v_1 and v_2 are DM velocities in the lab frame. $d\sigma_{3 \rightarrow 2}/dE_R$ is the differential cross section. The DM number density can be written as $n_{\text{DM}} = f(v) \rho_{\text{DM}} / m_{\text{DM}}$, where $f(v)$ is the DM velocity distribution function with $\int d^3 v f(v) = 1$ and $\rho_{\text{DM}} = 0.4 \text{ GeV}/\text{cm}^3$ being the local DM energy density [61]. Considering the fact that the recoil energy as well as the scattering amplitude are almost independent of the DM velocity, and assuming both DM particles and targets are unpolarized, one can absorb the factor $v_1 v_2$ in Eq. (1) into a cross section and integrate over velocities, resulting in a characteristic quantity, $\sigma_{3 \rightarrow 2} v^2$. Typically for the DM-electron scattering, the differential ionization rate is obtained by summing over electron from all possible (n, l) shells,

$$\frac{dR_{3 \rightarrow 2}}{dE_R} = \sum_{n,l} \frac{N_T \rho_{\text{DM}}^2 \langle \sigma(\mathbf{q}) v^2 \rangle}{4m_{\text{DM}}^2 E_R} |f_{\text{ion}}^{n,l}(k', \mathbf{q})|^2, \quad (2)$$

where we define a reference cross section $\langle \sigma(\mathbf{q}) v^2 \rangle \equiv \mathbf{q} |\mathcal{M}(\mathbf{q})|^2 / (32\pi m_{\text{DM}}^2 m_e E_e')$ and \mathbf{q}, E_e' denote the transfer momentum and the total energy of electron in final state. $f_{\text{ion}}^{n,l}(k', \mathbf{q})$ is the ionization form factor which plays crucial role in calculating bound electrons at low energy

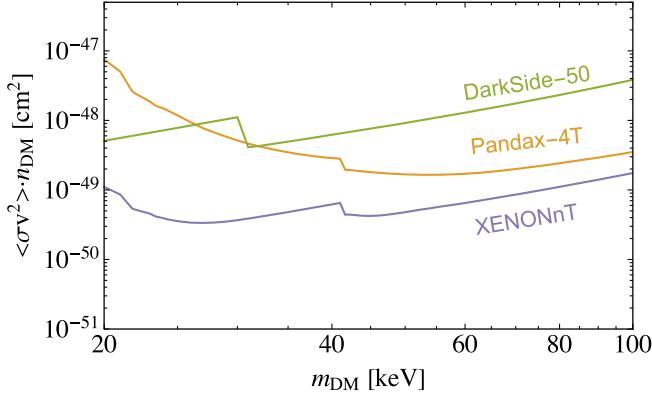


FIG. 2. Projected limits $\langle \sigma v^2 \rangle \cdot n_{\text{DM}}$ for XENONnT, PandaX-4T, and DarkSide-50 as a function of m_{DM} with xenon (argon)-based experiments.

scale [29,34,36,37]. The ionization form factor is calculated by using the Roothaan-Hartree-Fock radial wave function for the initial electron state and applying plane wave approximation for the final state (see Refs. [62,63] for detail).

In Fig. 2, we show the projected sensitivities to the ionization rate given in Eq. (2) for XENONnT [64] (purple), PandaX-4T [8] (orange), and DarkSide-50 (green) [65], respectively. We calculate the constraints on $\langle \sigma v^2 \rangle \cdot n_{\text{DM}}$ (cm²) for various m_{DM} over reported exposures (1.16 ton · year for XENONnT, 0.63 ton · year for PandaX-4T and 6786.0 kg · day for DarkSide-50) with a null signal event. The kinks in the plot correspond to the increase of ionized electrons as the transferred energy ΔE increases with the increase of m_{DM} . We note that detection efficiency may weaken the constraint and flatten some kinks at low energy transfer. We find that the limits induced by the $3 \rightarrow 2$ process is significant, which can be further applied to constrain parameter space of a specific DM model.

III. A TYPICAL MODEL

As an illustration, we study the direct detection signal of a complex scalar DM, $\Phi = \frac{1}{\sqrt{2}}(\chi + i\zeta)$, with additional gauge interaction $U(1)_D$, whose gauge field couples to the SM via the kinetic mixing with photon. Generally speaking, there is a mass splitting between χ and ζ arising from radiation corrections [66], leaving the lighter component as the DM candidate. Here we consider two scenarios: the real scalar χ being the DM, and the complex scalar Φ

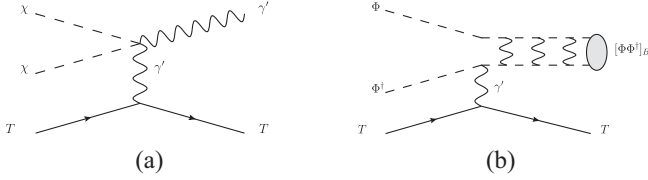
being the DM assuming negligible mass splitting between the CP -even and the CP -odd components. Relevant Lagrangians can be written as

$$\mathcal{L} \supset (D_\mu \Phi)^\dagger (D^\mu \Phi) + \frac{m_{A'}^2 (A'^\mu)^2}{2} + \epsilon e A'_\mu J_{\text{em}}^\mu, \quad (3)$$

where $D_\mu = \partial_\mu - i g_D A'_\mu$ is the covariant derivative with the new gauge coupling g_D , $m_{A'}$ is the mass of new gauge field, ϵ is the mixing parameter, J_{em}^μ is the electromagnetic current. Due to radiative corrections, the mass of ζ is usually different from that of χ , similar to the case of the inert DM [67], which means that the $2 \rightarrow 2$ inelastic scattering process $\chi + \text{SM} \rightarrow \zeta + \text{SM}$ can only occur in specific situations. The $2 \rightarrow 2$ elastic scattering process, $\chi + \text{SM} \rightarrow \chi + \text{SM}$, only exists at one-loop level due to the absence of a $\chi\chi A'$ interaction in the Lagrangian at the tree level. One-loop contributions to this process are suppressed by box diagrams. In addition, as shown in Fig. 1, for the DM with $\mathcal{O}(\text{GeV})$ scale mass, the recoil energy of the elastic scattering process $\Phi + \text{SM} \rightarrow \Phi + \text{SM}$ is of the order of $\mathcal{O}(\text{keV})$. Due to the limit of detector threshold, it is very difficult to detect such a signal in current xenon detectors if DM mass lies below GeV. All the facts above leave the $3 \rightarrow 2$ scattering process one possible way out for direct detection of MeV-scale DM. Two initial DMs scatter on target via a $3 \rightarrow 2$ process, $\text{DM} + \text{DM} + \text{T} \rightarrow \eta + \text{T}$, where η indicates one of the following final states: A' or $[\Phi\Phi^\dagger]_B$, and T denotes the target: electron or nuclei. Relevant Feynman diagrams are shown in Fig. 3. In the following, we will study the signal of these processes separately.

- (1) Scattering into DM bound state via the $3 \rightarrow 2$ process: If the dark photon mass is massless or much lighter than the DM, there is long-range interaction that typically implies the existence of DM bound states. We study the DM bound states in the nonrelativistic regime with nonconfining interactions. References [68,69] show that at lowest order in the coupling and in the nonrelativistic regime, the bound state formation cross sections do not depend on the spin configuration of the DM, therefore we consider the complex scalar DM case in bound state. As shown in the right panel of Fig. 3, DM may form bound state through the inelastic scattering process. The scattering amplitude can be written as

$$i\mathcal{M}(\Phi\Phi^\dagger\text{T} \rightarrow [\Phi\Phi^\dagger]_B\text{T}) = \sqrt{Z_{A'}(P_{A'})} \int \frac{d^4 p}{(2\pi)^4} \frac{d^4 k}{(2\pi)^4} \tilde{\Psi}_{P_n}^*(p) \tilde{\Phi}_{K_k}(k) \mathcal{A}^{(5)} \tilde{S}_{A'}(P_{A'}) i\mathcal{M}_{\text{SM}}. \quad (4)$$


 FIG. 3. Feynman diagrams of the $3 \rightarrow 2$ scattering process.

where $Z_{A'}(P_{A'})$ is the field-strength renormalization parameter for the mediator A' , $\Phi_{K,k}(k)$, and $\Psi_{P,n}(p)$ are the Bethe-Salpeter wave functions of DM in initial scattering states and final bound states, respectively. $\mathcal{A}^{(5)}(P_{A'}, p, k)$ is the five-point correlation function and $\tilde{S}_{A'}(P_{A'})$ is the propagator of A' [68]. $i\mathcal{M}_{\text{SM}}$ is the SM part amplitude. Note that the matrix element squared may depend on the scattering angle θ . Combining the general expression in Eq. (4) and the concrete interaction given by Eq. (3), the amplitude of $\Phi\Phi^\dagger e \rightarrow [\Phi\Phi^\dagger]_B e$ process at the leading order is derived in the Appendix A.

Assuming the initial two DM has the same mass, the energy transferred to the target particle can be expressed as

$$\Delta E = 2m_\Phi - \sqrt{\mathbf{q}^2 + M_{B\{n,l,m\}}^2}, \quad (5)$$

where $M_{B\{n,l,m\}}$ is the mass of final bound state at the $\{n, l, m\}$ level. For the capture in the final states $\{n, l, m\}$, the binding energy is [68]

$$\varepsilon_n = -\frac{\mu\alpha_D^2}{2n^2}, \quad (6)$$

where $\alpha_D = \frac{g_D^2}{4\pi}$, $\mu = \frac{1}{2}m_\Phi$ is the reduced mass of the DM pair. In order to ensure the sufficient efficiency of bound-state formation, we only consider the maximal value for $|\varepsilon_n|$ with $n = 1$. For the ground state $\{100\}$, the total energy of the bound state is $E_{B\{100\}} = \sqrt{\mathbf{q}^2 + M_{B\{100\}}^2}$ with its mass $M_{B\{100\}} = 2m_\Phi + \varepsilon_1$ [68]. So the transferred energy is roughly $|\varepsilon_1|$, which means that a larger binding energy results in a larger recoil energy.

(2) Scattering into dark photon via the $3 \rightarrow 2$ process: If $m_{A'} < 2m_\chi$ where $m_{A'}$ is the mass of dark photon, the inelastic $3 \rightarrow 2$ process, shown in the Fig. 3(a), is kinematically allowed and can be applied to search for DM in direct detection experiments, which has never been studied in any references. Assuming that the mass of dark photon is ultralight ($m_{A'} \ll m_\chi$), then the recoil energy for the target electron can be given by [29]

$$E_R \simeq 2m_\chi - q - |E_B^e|, \quad (7)$$

where E_B^e is the binding energy of electron in atom and q is the energy of dark photon. Substituting Eq. (7) and the squared matrix element given in Appendix B into Eq. (2), one obtains the whole expression for the rate of DM scattering off the electron. This process will be denoted as ‘‘scalar DM’’ in Fig. 4.

A. Constraints

Given the model, we present combined constraints on dark photon mass ($m_{A'}$) and the mixing parameter (ϵ) in Fig. 4. The slashed and horizontal lines denote the scalar and bound state DM, respectively. The solid, dashed and dotted lines correspond to 1, 10, 1000 ton \cdot year (t \cdot yr) exposures for the xenon and argon targets, respectively. The shaded region indicate a combination of cosmological, laboratorial, and astrophysical bounds, in which the light purple region describes the constraint of stellar cooling, the light blue region is the constraint from the cosmic microwave background spectrum [70] distorted by the $\gamma \rightarrow A'$ transition in the early Universe; the light orange region corresponds to the upper limits of viable dark photon DM from cosmological evolution [71–75], the middle and right green regions are the bounds from direct detection (XENON1T/XENON100 [76–78], WISPD MX [79] *et al.*), the gray band indicates the mass window from black holes

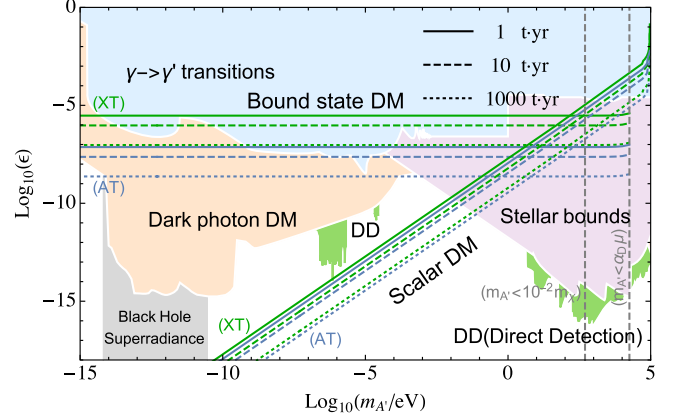


FIG. 4. Combined constraints on dark photon mass ($m_{A'}$) and the mixing parameter (ϵ). The slashed and horizontal lines denote the scalar DM and the bound state DM cases, where solid, dashed, and dotted lines indicate 1, 10, 1000 t \cdot yr scale exposure, respectively. The green and blue lines indicate the bounds from xenon and argon target detectors, respectively. As benchmark values, the DM mass is 50 keV and gauge coupling is $\alpha_D = 0.72$. Two gray dashed lines indicate the conditions for formation of bound state DM ($m_{A'} < \alpha_D \mu$) and $\xi \rightarrow 0$ ($m_{A'} \leq 10^{-2}m_\chi$) in scalar DM. The shaded region including various limits can be divided into three categories based on cosmological (orange), experimental (blue, green), and astrophysical (pink) bounds. The gray band indicates the constraint from black holes super-radiance.

superradiance [80]. A more detailed description of each bound can be found in a recent review [81] and references therein.

In evaluating constraints of $3 \rightarrow 2$ DM-electron scattering, we set the DM mass and the gauge coupling as $m_{\text{DM}} = 50 \text{ keV}$ and $\alpha_D = 0.72$, and further apply the detection efficiencies and thresholds of XENONnT [64] and DarkSide-50 [65] to generate limits for the xenon and argon detectors for illustration. For this benchmark, the spectrum of the bound state DM is very different from that of the scalar DM. For the bound state DM, the squared matrix and the limits are almost independent of $m_{A'}$, as can be seen from Eq. (B2) in Appendix B, and the condition for bound state ($m_{A'} < \alpha_D \mu$) should be satisfied [68], which results in a truncation at the right end of the limits. Considering the fact that the recoil energy is about 1 keV and the threshold of the argon detector is much lower than that of xenon detector, the constraint of argon detector is more stringent, which may cover regimes not involved in indirect detections for future projected argon experiment. For scalar DM, where we use a hard cutoff ($m_{A'} \leq 10^{-2} m_\chi$) to match the $\xi \rightarrow 0$ condition, the shape of the spectrum comes from the fact that the squared matrix is proportional to $m_{A'}^{-2}$. Given the recoil energy induced by $3 \rightarrow 2$ DM-electron scattering, which is about 8 keV for the benchmark, the limits are much more stringent than those from traditional direct and indirect detections even for the existed exposure of XENONnT at around 1 t · yr.

Before proceeding to further studies, we comment on the relic density of dark matter models presented in this paper as follows: For the real scalar dark matter, it may be generated either from the freeze-out mechanism or from the freeze-in mechanism in the early Universe. The relic density can be determined by the general $2 \rightarrow 2$ annihilation processes in the freeze-out mechanism, while it can also be generated from the decay of the mother particle, which is in the thermal bath, via kinetic mixing in the freeze-in mechanism. For the dark matter model that may form a composite state, it can be generated from the decay of the mother particle in the hidden sector, which is not in the thermal bath. For example, given the following Yukawa interaction in the hidden sector: $y\bar{\chi}\Phi\eta + \text{H.c.}$, and further assuming η mixes with active neutrinos, then the decay process $\chi \rightarrow \Phi\nu$ may lead to the single production of Φ in the early Universe. In this way, there exists free scalar dark matter that does not form a composite state nowadays. It should be mentioned that the $3 \rightarrow 2$ annihilation processes may also contribute to the relic abundance, similar to conventional SIMP cases, but their effects can be subdominated in our studies. In short, the relic density of dark matter models presented in this paper may be determined by extra interactions in the dark sector, and the interactions given in Eq. (3) are mainly relevant to the direct detection signal.

IV. $3 \rightarrow 2$ DM-NUCLEI SCATTERING

DM-nuclei scattering has been a promising channel for DM direct detections and it already put strong constraint on weakly interacting massive particle (WIMP)-nuclei interactions. However this constraint dramatically weakens for DM mass smaller than about 1 GeV. This is due to the rapidly decreasing sensitivity at low recoil energies. The traditional DM-nuclei scattering leaves light DM candidates poorly explored by direct searches. Several approaches have been proposed to directly detect DM at this mass range, such as inelastic DM-nuclei scattering [82] and boosted DM, where a fraction of DM gets a high velocity due to a number of mechanisms [83]. The model independent constraint on the DM-nucleon cross section is about 10^{-31} cm^2 for cosmic ray boosted DM. In this section we consider the possibility of detecting sub-MeV DM via the $3 \rightarrow 2$ process. Taking scalar DM as an example, the Feynman diagram is given in the left panel of Fig. 3 and the $\sigma_{3 \rightarrow 2}^{\text{DMN}} v^2$ can be written as $\sigma_{3 \rightarrow 2}^{\text{DMN}} v^2 \approx \frac{q_0}{32\pi m_{\text{DM}}^2 m_N^2} |\mathcal{M}|^2 * C_N^2$, where $|\mathcal{M}|^2$ is the squared matrix element whose expression is exactly given in Appendix B up to replacement $m_e \leftrightarrow m_N$, $C_N = 2c_u^p + c_d^p$ being the matching factor from the quark level to nucleon level, $q_0 \simeq \sqrt{4 - \xi^2} m_{\text{DM}}$ being the momentum transfer.

References [27,28] have studied the absorption of a Fermionic DM in direct detection, where the energy transfer equals a dark matter mass. Here we are the first of studying the signal of the $3 \rightarrow 2$ inelastic scattering process in nuclei. The total rate for multiple nuclei can be written as

$$R = \left(\frac{\rho_{\text{DM}}}{m_{\text{DM}}} \right)^2 \sigma_{3 \rightarrow 2}^{\text{DMN}} v^2 \sum_i N_{T,i} Z_i^2 F_i^2 \Theta(E_{R,i}^0 - E_{\text{th}}), \quad (8)$$

where $\sigma_{3 \rightarrow 2}^{\text{DMN}} v^2$ is the reduced $3 \rightarrow 2$ inelastic cross section per nucleon, Z_i is the atomic number for i th target nuclei,

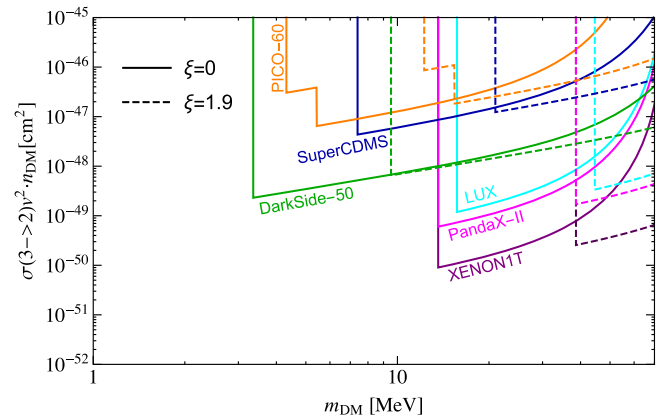


FIG. 5. Limits of several current experiments to $\sigma_{3 \rightarrow 2} v^2 \cdot n_{\text{DM}}$ versus m_{DM} . The solid and dashed lines denote $\xi = 0, 1.9$, which correspond to scattering into dark photon and bound state final states, respectively. The exposures of several direct detection experiments are listed in the Table II.

F is the Helm form factor [84]. The recoil energy of nuclei is monoenergetic and the signature is peaked at $E_R = E_R^0 \simeq (4 - \xi^2)m_{\text{DM}}^2/(2m_A)$. E_{th} is the threshold of direct detection, which is based on the following experiments' thresholds. Figure 5 shows the projected sensitivities on $\sigma_{3 \rightarrow 2}^{\text{DMN}} v^2 \cdot n_{\text{DM}}$ as a function of m_{DM} in various direct detection experiments including LUX [55], PandaX-II [56], XENON1T [57], PICO-60(C₃F₈) [85], SuperCDMS [7], and DarkSide-50 [5], where the solid and dashed lines correspond to scalar DM and bound state DM cases with $\xi = 0$ and 1.9, respectively. We use the exposure for various experiments listed in Table II of Appendix E and further assume null direct detection signal ($R \leq 2.7$) to derive the limits.

V. CONCLUSION

Direct detection of DM in underground laboratories has been a promising way of exploring the particle nature of DM. Given the situation that all searches of WIMPs have turned up null even for exponentially increased exposure, direct detection of sub-MeV DM becomes more and more relevant, even though the detection ability is weak due to the limitation of the detector threshold. In this paper, we have proposed a new direct detection strategy via a 3-body inelastic scattering process. The energy transfer to the detector target in this process is enhanced compared with the $2 \rightarrow 2$ scattering process, so it can be applied to the

direct detection of lighter DM. We have extracted the generic physical observable for this process and presented its effects in the direct detection of complex scalar DM. It should be mentioned that this method is also applicable to the direct detection of fermion DM.

ACKNOWLEDGMENTS

We thank Qian-Fei Xiang for useful discussions. This work was supported by the National Natural Science Foundation of China under Grants No. 11775025 and No. 12175027.

APPENDIX A: DERIVATION OF THE SCATTERING AMPLITUDE IN A BOUND STATE

Following the quantum-field-theoretical procedure in Ref. [68], the leading-order contribution of the entire $\Phi\Phi^\dagger e \rightarrow [\Phi\Phi^\dagger]_B e$ scattering is shown in Fig. 6, where q_1, q_2 , and p_1, p_2 are the momenta of the dark matter in the scattering states and the bound states, q_3, p_3 , and $P_{A'}$ are the momenta of the initial electron, the final electron and the dark photon, respectively. “ $-\bullet-$ ” denotes the full propagators of dark matter. Without loss of generality, we denote the coupling coefficients of the initial DMs with the dark photon as g_1, g_2 , respectively. Then the contribution of Fig. 6 is evaluated to be

$$\begin{aligned} & (2\pi)^4 \delta^4(q_1 + q_2 + q_3 - p_1 - p_2 - p_3) i C_{A'-\text{amp}}^{(5)\mu} \tilde{S}_{A'}(p_3 - q_3) [\bar{u}(p_3)(-ie\gamma^\nu)u(q_3)] \\ & \simeq \{ -ig_1(p_1^\mu + q_1^\mu) \tilde{S}_1(p_1) \tilde{S}_1(q_1) (2\pi)^4 \delta^4(p_3 - q_3 + p_1 - q_1) \tilde{S}_2(q_2) (2\pi)^4 \delta^4(p_2 - q_2) \tilde{S}_{A'}(p_3 - q_3) [\bar{u}(p_3)(-ie\gamma^\nu)u(q_3)] \\ & \quad - ig_2(p_2^\mu + q_2^\mu) \tilde{S}_2(p_2) \tilde{S}_2(q_2) (2\pi)^4 \delta^4(p_3 - q_3 + p_2 - q_2) \tilde{S}_1(q_1) (2\pi)^4 \delta^4(p_1 - q_1) \tilde{S}_{A'}(p_3 - q_3) [\bar{u}(p_3)(-ie\gamma^\nu)u(q_3)] \}, \end{aligned} \quad (\text{A1})$$

where $C_{A'-\text{amp}}^{(5)\mu} = C_{A'-\text{amp}}^{(5)\mu}(P_{A'}, p_1, p_2, q_1, q_2)$. We define

$$\eta_{1,2} = \frac{m_{1,2}}{m_1 + m_2} \quad (\text{A2})$$

and

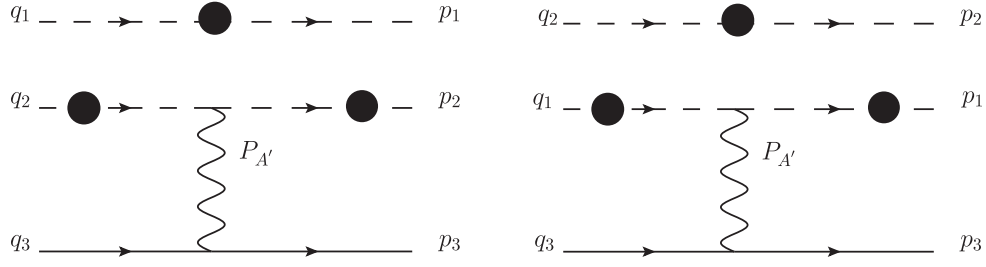
$$\begin{aligned} p_1 &= \eta_1 P + p, & q_1 &= \eta_1 K + k, \\ p_2 &= \eta_2 P - p, & q_2 &= \eta_2 K - k, \end{aligned} \quad (\text{A3})$$

where P, p and K, k are the conjugate momenta of the relevant coordinates, see Chapter 3.1 in Ref. [68] for details. The conservation of 4-momentum gives

$$K + q_3 = P + p_3, \quad K = P + P_{A'}. \quad (\text{A4})$$

Integrating q_3 on both sides of Eq. (A1) and then substituting Eqs. (A3), (A4) into it, which leads to

$$\begin{aligned} & C_{A'-\text{amp}}^{(5)\mu} \tilde{S}_{A'}(P_{A'}) [\bar{u}(p_3)(-ie\gamma^\nu)u(p_3 - P_{A'})] \\ & \simeq -g_1 S(k; K) [2\eta_1 K^\mu - (\eta_1 - \eta_2) P_{A'}^\mu + 2p^\mu] \tilde{S}_1(\eta_1 P + p) (2\pi)^4 \delta^4(k - p - \eta_2 P_{A'}) \tilde{S}_{A'}(P_{A'}) [\bar{u}(p_3)(-ie\gamma^\nu)u(p_3 - P_{A'})] \\ & \quad - g_2 S(k; K) [2\eta_2 K^\mu + (\eta_1 - \eta_2) P_{A'}^\mu - 2p^\mu] \tilde{S}_2(\eta_2 P - p) (2\pi)^4 \delta^4(k - p + \eta_1 P_{A'}) \tilde{S}_{A'}(P_{A'}) [\bar{u}(p_3)(-ie\gamma^\nu)u(p_3 - P_{A'})], \end{aligned} \quad (\text{A5})$$

FIG. 6. The leading-order contribution of the entire $\Phi\Phi^\dagger e \rightarrow [\Phi\Phi^\dagger]_B e$ process.

where $\mathcal{C}_{A'\text{-amp}}^{(5)\mu} = \mathcal{C}_{A'\text{-amp}}^{(5)\mu}(P_{A'}, \eta_1 K + k, \eta_2 K - k, \eta_1 P + p, \eta_2 P - p)$, $\tilde{S}_{A'}(P_{A'}) = \frac{-ig_{\mu\nu}}{P_{A'}^2 - m_{A'}^2}$ is the propagator, and we have used the definition [68]

$$S(k; K) = \tilde{S}_1(q_1)\tilde{S}_2(q_2). \quad (\text{A6})$$

For convenience, we define

$$\begin{aligned} \mathcal{C}_{A'\text{-amp}}^{(5)\mu} \tilde{S}_{A'}(P_{A'}) [\bar{u}(p_3)(-ie\epsilon\gamma^\nu)u(p_3 - P_{A'})] \\ = \mathcal{M}_{\text{trans}}^\mu [\bar{u}(p_3)\gamma_\mu u(p_3 - P_{A'})], \end{aligned} \quad (\text{A7})$$

from Eq. (A5), we find

$$\begin{aligned} \mathcal{M}_{\text{trans}}^\mu = \frac{eeS(k; K)}{P_{A'}^2 - m_{A'}^2} \left\{ g_1 [2\eta_1 K^\mu - (\eta_1 - \eta_2)P_{A'}^\mu + 2p^\mu] \tilde{S}_1(\eta_1 P + p) (2\pi)^4 \delta^4(k - p - \eta_2 P_{A'}) \right. \\ \left. + g_2 [2\eta_2 K^\mu + (\eta_1 - \eta_2)P_{A'}^\mu - 2p^\mu] \tilde{S}_2(\eta_2 P - p) (2\pi)^4 \delta^4(k - p + \eta_1 P_{A'}) \right\}. \end{aligned} \quad (\text{A8})$$

Using the approximate result of $\mathcal{M}_{\text{trans}}^\mu(\vec{p}, \vec{k})$ calculated in Ref. [68]

$$\mathcal{M}_{\text{trans}}^\mu(\vec{p}, \vec{k}) = \frac{1}{\mathcal{S}_0(\vec{k}; K)\mathcal{S}_0(\vec{p}; P)} \int \frac{d^0 p}{2\pi} \int \frac{d^0 k}{2\pi} \mathcal{M}_{\text{trans}}^\mu, \quad (\text{A9})$$

and substituting Eq. (A8) into Eq. (A9), we obtain

$$\begin{aligned} \mathcal{M}_{\text{trans}}^\mu(\vec{p}, \vec{k}) = \frac{ee}{P_{A'}^2 - m_{A'}^2} \frac{1}{\mathcal{S}_0(\vec{k}; K)\mathcal{S}_0(\vec{p}; P)} \left\{ g_1 [2\eta_1 K^\mu - (\eta_1 - \eta_2)P_{A'}^\mu + 2p^\mu] \Xi_1(\vec{k}, \vec{p}; K, P) (2\pi)^3 \delta^3(\vec{k} - \vec{p} - \eta_2 \vec{P}_{A'}) \right. \\ \left. + g_2 [2\eta_2 K^\mu + (\eta_1 - \eta_2)P_{A'}^\mu - 2p^\mu] \Xi_2(\vec{k}, \vec{p}; K, P) (2\pi)^3 \delta^3(\vec{k} - \vec{p} + \eta_1 \vec{P}_{A'}) \right\}, \end{aligned} \quad (\text{A10})$$

where the forms of Ξ_1 , Ξ_2 and their nonrelativistic approximations can be found in Chapter 5 of Ref. [68]. Then the transition amplitude can be expressed in terms of the Schrödinger wave functions

$$\mathcal{M}_{\vec{k} \rightarrow n}^i \simeq \sqrt{2\mu} \int \frac{d^3 p}{(2\pi)^3} \frac{d^3 k}{(2\pi)^3} \frac{\tilde{\psi}_n^*(\vec{p}) \tilde{\phi}_{\vec{k}}(\vec{q})}{\sqrt{2\mathcal{N}_{\vec{p}}(\vec{p}) 2\mathcal{N}_{\vec{k}}(\vec{k})}} \mathcal{M}_{\text{trans}}^i(\vec{k}; \vec{p}), \quad (\text{A11})$$

where

$$\frac{1}{\sqrt{2\mathcal{N}_{\vec{p}}(\vec{p}) 2\mathcal{N}_{\vec{k}}(\vec{k})}} \simeq \frac{1}{2\mu} \left[1 - \frac{\vec{p}^2 + \vec{k}^2}{4\mu^2} \left(1 - \frac{3\mu}{M} \right) \right], \quad (\text{A12})$$

and

$$\mu = \frac{m_1 m_2}{m_1 + m_2}, \quad M = m_1 + m_2, \quad (\text{A13})$$

are the reduced and the total masses of the initial DMs, respectively.

Substituting Eqs. (A10)–(A13) into Eq. (A11), the transition amplitude is changed to be

$$\begin{aligned} \mathcal{M}_{k \rightarrow n}^i &\simeq \sqrt{2\mu} \int \frac{d^3 p}{(2\pi)^3} \frac{d^3 k}{(2\pi)^3} \tilde{\psi}_n^*(\vec{p}) \tilde{\phi}_{\vec{k}}(\vec{k}) \frac{1}{2\mu} \left[1 - \frac{\vec{p}^2 + \vec{k}^2}{4\mu^2} \left(1 - \frac{3\mu}{M} \right) \right] \frac{\epsilon e}{P_{A'}^2 - m_{A'}^2} \\ &\times \left\{ g_1 [2\eta_1 K^i - (\eta_1 - \eta_2) P_{A'}^i + 2p^i] 2m_2 \left[1 + \frac{\vec{p}^2}{2\mu^2} \left(1 - \frac{2\mu}{M} \right) \right] (2\pi)^3 \delta^3(\vec{k} - \vec{p} - \eta_2 \vec{P}_{A'}) \right. \\ &\left. + g_2 [2\eta_2 K^i + (\eta_1 - \eta_2) P_{A'}^i - 2p^i] 2m_1 \left[1 + \frac{\vec{p}^2}{2\mu^2} \left(1 - \frac{2\mu}{M} \right) \right] (2\pi)^3 \delta^3(\vec{k} - \vec{p} + \eta_1 \vec{P}_{A'}) \right\}, \end{aligned} \quad (\text{A14})$$

we only keep the leading-order contribution in p and integrate k out, then Eq. (A14) is reduced to

$$\begin{aligned} \mathcal{M}_{k \rightarrow n}^i &\simeq \sqrt{2\mu} \frac{\epsilon e}{P_{A'}^2 - m_{A'}^2} \int \frac{d^3 p}{(2\pi)^3} \tilde{\psi}_n^*(\vec{p}) \left\{ g_1 \left[2\eta_1 K^i - (\eta_1 - \eta_2) P_{A'}^i + 2p^i \right] \frac{m_2}{\mu} \tilde{\phi}_{\vec{k}}(\vec{p} + \eta_2 \vec{P}_{A'}) \right. \\ &\left. + g_2 \left[2\eta_2 K^i + (\eta_1 - \eta_2) P_{A'}^i - 2p^i \right] \frac{m_1}{\mu} \tilde{\phi}_{\vec{k}}(\vec{p} - \eta_1 \vec{P}_{A'}) \right\}. \end{aligned} \quad (\text{A15})$$

Some useful integrals are introduced in Ref. [68]

$$\mathcal{I}_{\vec{k},n}(\vec{b}) \equiv \int \frac{d^3 p}{(2\pi)^3} \tilde{\psi}_n^*(\vec{p}) \tilde{\phi}_{\vec{k}}(\vec{p} + \vec{b}), \quad (\text{A16})$$

$$\vec{\mathcal{J}}_{\vec{k},n}(\vec{b}) \equiv \int \frac{d^3 p}{(2\pi)^3} \vec{p} \tilde{\psi}_n^*(\vec{p}) \tilde{\phi}_{\vec{k}}(\vec{p} + \vec{b}), \quad (\text{A17})$$

we can reexpress Eq. (A14) in terms of these integrals as follows:

$$\begin{aligned} \mathcal{M}_{k \rightarrow n}^j &= 2\sqrt{2\mu} \frac{\epsilon e}{P_{A'}^2 - m_{A'}^2} \left\{ \frac{g_1}{\eta_1} \mathcal{J}_{\vec{k},n}^j(\eta_2 \vec{P}_{A'}) - \frac{g_2}{\eta_2} \mathcal{J}_{\vec{k},n}^j(-\eta_1 \vec{P}_{A'}) \right. \\ &\left. + \left[g_1 \left(K^j - \frac{\eta_1 - \eta_2}{2\eta_1} P_{A'}^j \right) \mathcal{I}_{\vec{k},n}(\eta_2 \vec{P}_{A'}) + g_2 \left(K^j + \frac{\eta_1 - \eta_2}{2\eta_2} P_{A'}^j \right) \mathcal{I}_{\vec{k},n}(-\eta_1 \vec{P}_{A'}) \right] \right\}. \end{aligned} \quad (\text{A18})$$

Finally, according to the dark matter bound-state formation amplitude in Eq. (A18), the total scattering amplitude squared of the $\Phi\Phi^\dagger e \rightarrow [\Phi\Phi^\dagger]_B e$ process can be obtained

$$\begin{aligned} |\overline{\mathcal{M}}_{k \rightarrow n}^j|^2 &= \frac{1}{2} \sum_{\text{spin}} \left| \mathcal{M}_{k \rightarrow n}^\mu \bar{u}(p_3) \gamma_\mu u(p_3 - P_{A'}) \right|^2, \\ &= \mathcal{M}_{k \rightarrow n}^\mu (\mathcal{M}_{k \rightarrow n}^\nu)^* \left[2g_{\mu\nu} (P_{A'} \cdot p_3) - 2P_{A'\nu} p_{3\mu} - 2P_{A'\mu} p_{3\nu} + 4p_{3\mu} p_{3\nu} \right]. \end{aligned} \quad (\text{A19})$$

The Ward-Takahashi identity tells us that

$$\begin{aligned} (P_{A'})_\mu \mathcal{M}_{k \rightarrow n}^\mu(P_{A'}; q_1, q_2; p_1, p_2) &= g_1 \sum_{i=1}^2 [\mathcal{M}_0(P_{A'}; q_1, q_2; p_i - P_{A'}) - \mathcal{M}_0(P_{A'}; q_i + P_{A'}; p_1, p_2)] \\ &\quad + g_2 \sum_{i=1}^2 [\mathcal{M}_0(P_{A'}; q_1, q_2; p_i - P_{A'}) - \mathcal{M}_0(P_{A'}; q_i + P_{A'}; p_1, p_2)], \\ &= (g_1 + g_2) \sum_{i=1}^2 [\mathcal{M}_0(P_{A'}; q_1, q_2; p_i - P_{A'}) - \mathcal{M}_0(P_{A'}; q_i + P_{A'}; p_1, p_2)]. \end{aligned} \quad (\text{A20})$$

For the attractive DM interaction,

$$g_1 g_2 < 0. \quad (\text{A21})$$

In the case of a identical dark matter pair, we have

$$m_1 = m_2 = m_\Phi, \quad (\text{A22})$$

then μ , η_1 , η_2 , and g_1 , g_2 can be obtained:

$$\eta_1 = \eta_2 = \frac{1}{2}, \quad (\text{A23})$$

$$\mu = \frac{m_\Phi}{2}, \quad (\text{A24})$$

$$g_1 = -g_2 = g_D. \quad (\text{A25})$$

The Ward-Takahashi identity in Eq. (A20) is reduced to

$$(P_{A'})_\mu \mathcal{M}_{k \rightarrow n}^\mu(P_{A'}; q_1, q_2; p_1, p_2) = 0, \quad (\text{A26})$$

which is known as the Ward identity. According to the Ward identity, the 0 component of dark matter bound-state formation amplitude can be written as

$$\mathcal{M}_{k \rightarrow n}^0 = \frac{P_{A'}^i \mathcal{M}_{k \rightarrow n}^i}{P_{A'}^0}. \quad (\text{A27})$$

Therefore, we can express the total scattering amplitude squared in the form that only contains $i, j(1, 2, 3)$ components,

$$\begin{aligned} |\overline{\mathcal{M}_{k \rightarrow n}^0}|^2 &= 2(P_{A'} \cdot p_3) \left[\frac{|P_{A'}^i \mathcal{M}_{k \rightarrow n}^i|^2}{(P_{A'}^0)^2} - \mathcal{M}_{k \rightarrow n}^j (\mathcal{M}_{k \rightarrow n}^j)^* \right] + 4 \left[(p_3^0)^2 \frac{|P_{A'}^i \mathcal{M}_{k \rightarrow n}^i|^2}{(P_{A'}^0)^2} \right. \\ &\quad \left. - \frac{p_3^0}{P_{A'}^0} (P_{A'}^j \mathcal{M}_{k \rightarrow n}^j)^* (p_3^i \mathcal{M}_{k \rightarrow n}^i) - \frac{p_3^0}{P_{A'}^0} (p_3^j \mathcal{M}_{k \rightarrow n}^{j*}) (P_{A'}^i \mathcal{M}_{k \rightarrow n}^i) + (p_3^j \mathcal{M}_{k \rightarrow n}^{j*}) (p_3^i \mathcal{M}_{k \rightarrow n}^i) \right]. \quad (\text{A28}) \end{aligned}$$

Following the calculations in Ref. [68], for the capture in the ground state $\{100\}$, we keep only the leading-order terms for $\mathcal{I}_{\vec{k}, \{100\}}$ and $\mathcal{J}_{\vec{k}, \{100\}}$,

$$\vec{\mathcal{I}}_{\vec{k}, \{100\}}(\vec{b}) \simeq \frac{2\mathcal{R}(\zeta)}{1 + \zeta^2} \frac{b}{k^{5/2}} \cos \tilde{\theta}, \quad (\text{A29})$$

$$\vec{\mathcal{J}}_{\vec{k}, \{100\}}(\vec{b}) \simeq \frac{\mathcal{R}(\zeta)}{k^{3/2}} \vec{k}, \quad (\text{A30})$$

and the parameters θ and \vec{b} are defined as

$$\cos \theta = \frac{\vec{k} \cdot \vec{P}_{A'}}{|\vec{k}| |\vec{P}_{A'}|}, \quad (\text{A31})$$

with

$$\tilde{\theta} = \begin{cases} \theta, & \text{for } \vec{b} = \eta_2 \vec{P}_{A'} \\ \pi + \theta, & \text{for } \vec{b} = -\eta_1 \vec{P}_{A'} \end{cases}, \quad (\text{A32})$$

and other parameters can be found in Ref. [68].

Under the above conditions, the dark matter bound-state formation amplitude in Eq. (A18) is approximated to be

$$\begin{aligned} \mathcal{M}_{k \rightarrow \{100\}}^j &= 2\sqrt{2\mu} \frac{ee}{P_{A'}^2 - m_{A'}^2} \left\{ (g_1 - g_2) \frac{2\mathcal{R}(\zeta)}{|\vec{k}|^{3/2}} k^j \sin \theta \right. \\ &\quad \left. + (g_1 - g_2) \frac{\mathcal{R}(\zeta)}{(1 + \zeta^2)} \frac{|\vec{P}_{A'}|}{|\vec{k}|^{5/2}} K^j \cos \theta \right\}. \quad (\text{A33}) \end{aligned}$$

We calculate the total scattering amplitude in the rest frame of dark matter and electron. The relevant 4-momenta are given by

$$\begin{aligned} K &= (2m_\Phi, 0), & k &= (0, \mu \vec{v}_{\text{rel}}), & q_3 &= (m_e, \vec{0}), \\ P &= (E_B, -\vec{q}), & p_3 &= (E_e', \vec{q}), \end{aligned} \quad (\text{A34})$$

the relative velocity \vec{v}_{rel} in k is not negligible due to the nonsingularity of the dimensionless parameter $\zeta = \frac{\alpha_D}{|\vec{v}_{\text{rel}}|}$. Then the amplitude in Eq. (A33) is reduced to

$$\mathcal{M}_{k \rightarrow \{100\}}^j = 2\sqrt{2\mu} \frac{ee}{P_{A'}^2 - m_{A'}^2} \left\{ (2g_D) \frac{2\mathcal{R}(\zeta)}{|\vec{k}|^{3/2}} k^j \sin \theta \right\}. \quad (\text{A35})$$

APPENDIX B: THE MATRIX ELEMENT SQUARED FOR DM-ELECTRON SCATTERING

In this section we calculate the analytical expressions of matrix elements squared of DM-electron scattering for dark photon and bound final states. According to Feynman diagrams in Fig. 3, the matrix element squared for scalar DM is

$$\overline{|\mathcal{M}|^2}_S = \frac{64\pi\alpha g_D^4 m_e \epsilon^2 [2m_\chi E_{A'}(m_\chi + m_e) - m_{A'}^2(E_{A'} - m_\chi + m_e)]}{m_{A'}^2(-2m_e E_{A'} + m_{A'}^2 + 4m_\chi m_e)^2}, \quad (\text{B1})$$

where the total energy of dark photon $E_{A'} = \sqrt{m_{A'}^2 + q^2} \simeq q$. For the bound state DM, combining Eqs. (A28), (A34), and (A35), we obtain

$$\begin{aligned} \overline{|\mathcal{M}_{\vec{k} \rightarrow \{100\}}|^2} &= \frac{\epsilon^2 e^2 (2g_D)^2}{\left[-4m_e m_\Phi + 2m_e \sqrt{\vec{q}^2 + M_{B\{100\}}^2} - m_{A'}^2\right]^2} \frac{64}{|\vec{v}_{\text{rel}}|} |\mathcal{R}(\xi)|^2 \\ &\times \left\{ \left((2m_\Phi - E_{B\{100\}})E'_e - \vec{q}^2 \right) \left[\frac{\vec{q}^2 \cos^2 \theta \sin^2 \theta}{(2m_\Phi - E_{B\{100\}})^2} - \sin^2 \theta \right] \right. \\ &\left. + 2(E'_e)^2 \left[\frac{\vec{q}^2 \cos^2 \theta \sin^2 \theta}{(2m_\Phi - E_{B\{100\}})^2} \right] - \frac{4E'_e}{2m_\Phi - E_{B\{100\}}} \vec{q}^2 \cos^2 \theta \sin^2 \theta + 2\vec{q}^2 \cos^2 \theta \sin^2 \theta \right\}. \quad (\text{B2}) \end{aligned}$$

APPENDIX C: DIFFERENTIAL IONIZATION RATE FOR DM-ELECTRON SCATTERING

The cross section for the $3 \rightarrow 2$ process is written as follows:

$$\langle \sigma v^2 \rangle = \frac{1}{4E_{A'} E'_e} \int \frac{d^3 q}{(2\pi)^3} \frac{d^3 k'}{(2\pi)^3} \frac{1}{8E_{\text{DM}}^2 E_e} (2\pi)^4 \delta(E_i - E_f) \delta^3(\vec{k} + \vec{q} - \vec{k}') \overline{|\mathcal{M}(q)|^2} \times |f(\vec{q})|^2, \quad (\text{C1})$$

$$= \frac{1}{32E_{A'} E'_e E_{\text{DM}}^2 E_e} \int \frac{d^3 q}{(2\pi)^3} 2\pi \delta(\Delta E - 2m_{\text{DM}} + \sqrt{q^2 + m_{A'}^2}) \overline{|\mathcal{M}(q)|^2} |f(\vec{q})|^2. \quad (\text{C2})$$

Following the procedure in Ref. [29], the event rate is derived by

$$R = N_T \left(\frac{\rho_{\text{DM}}}{m_{\text{DM}}} \right)^2 \int d^3 v g_{\text{DM}}(v) \langle \sigma v^2 \rangle, \quad (\text{C3})$$

$$= \frac{N_T \rho_{\text{DM}}^2}{32m_{\text{DM}}^2 E_{A'} E'_e E_e E_{\text{DM}}^2} \int \frac{d^3 q}{(2\pi)^2} d^3 v g_{\text{DM}}(v) \delta(\Delta E - 2m_{\text{DM}} + \sqrt{q^2 + m_{A'}^2}) \overline{|\mathcal{M}(q)|^2} |f(\vec{q})|^2, \quad (\text{C4})$$

$$= \frac{N_T \rho_{\text{DM}}^2}{32m_{\text{DM}}^2 E_{A'} E'_e E_e E_{\text{DM}}^2} \int \frac{d^3 q}{(2\pi)^2} \delta(\Delta E - 2m_{\text{DM}} + \sqrt{q^2 + m_{A'}^2}) \overline{|\mathcal{M}(q)|^2} |f(\vec{q})|^2, \quad (\text{C5})$$

where $g_{\text{DM}}(\vec{v})$ is the distribution function of dark matter velocity. After replacing the form factor $f(q) \rightarrow f_{\text{ion}}(k', q)$ in Eq. (C5) by applying the Eq. (A.21) from Ref. [29], we integrate q and then the differential ionization rate is written as

$$\frac{dR_{3 \rightarrow 2}}{dE_R} = \sum_{n,l} \frac{N_T \rho_{\text{DM}}^2}{128\pi m_{\text{DM}}^4 m_e E'_e E_R} q \overline{|\mathcal{M}(q)|^2} |f_{\text{ion}}^{n,l}(k', q)|^2, \quad (\text{C6})$$

where we take the approximation $E_{\text{DM}} \approx m_{\text{DM}}$, $E_e \approx m_e$.¹ $E'_e = m_e + 2m_{\text{DM}} - \sqrt{q^2 + m_{A'}^2}$, $E_{A'} = \sqrt{q^2 + m_{A'}^2} \simeq q$, $k' = \sqrt{2m_e E_R}$, where E_R is the recoil energy of electron.

¹The initial electron should be described by $E_e = m_e - E_B$ where E_B is the binding energy of atomic electron. Since the $E_B \ll m_e$, thus we take the approximation $E_e \approx m_e$ for convenience.

APPENDIX D: BINDING ENERGY FOR XENON ELECTRON SHELLS

TABLE I. Binding energy for xenon electron shells [54].

(n, l) shell	$5p^6$	$5s^2$	$4d^{10}$	$4p^6$	$4s^2$	$3d^{10}$
$ E_B^{nl} $ [eV]	12.4	25.7	75.6	163.5	213.8	710.7
(n, l) shell	$3p^6$	$3s^2$	$2p^6$	$2s^2$	$1s^2$	
$ E_B^{nl} $ [eV]	958.4	1093.2	4837.7	5152.2	33317.6	

APPENDIX E: THE EXPOSURE OF SEVERAL EXPERIMENTS

TABLE II. The exposure of several experiments [27].

Detector	LUX	PandaX-II	XENON1T	PICO-60(C ₃ F ₈)	SuperCDMS	DarkSide-50
Exposure	91.8 kg yr	150 kg yr	1.0 t yr	1167 kg day	577 kg day	6786 kg day

-
- [1] J. Liu, X. Chen, and X. Ji, *Nat. Phys.* **13**, 212 (2017).
[2] T. Lin, *Proc. Sci.* 333 (2019) 009.
[3] K. Griest and M. Kamionkowski, *Phys. Rev. Lett.* **64**, 615 (1990).
[4] G. Steigman and M. S. Turner, *Nucl. Phys.* **B253**, 375 (1985).
[5] P. Agnes *et al.* (DarkSide Collaboration), *Phys. Rev. Lett.* **121**, 081307 (2018).
[6] E. Aprile *et al.* (XENON Collaboration), *Phys. Rev. Lett.* **121**, 111302 (2018).
[7] R. Agnese *et al.* (SuperCDMS Collaboration), *Phys. Rev. Lett.* **112**, 241302 (2014).
[8] Y. Meng *et al.* (PandaX-4T Collaboration), *Phys. Rev. Lett.* **127**, 261802 (2021).
[9] W. Chao, T. Li, and J. Liao, arXiv:2108.05608.
[10] A. Das and M. Sen, *Phys. Rev. D* **104**, 075029 (2021).
[11] Y. Jho, J.-C. Park, S. C. Park, and P.-Y. Tseng, arXiv:2101.11262.
[12] L. Su, W. Wang, L. Wu, J. M. Yang, and B. Zhu, *Phys. Rev. D* **102**, 115028 (2020).
[13] B. Fornal, P. Sandick, J. Shu, M. Su, and Y. Zhao, *Phys. Rev. Lett.* **125**, 161804 (2020).
[14] H. An and D. Yang, *Phys. Lett. B* **818**, 136408 (2021).
[15] H.-J. He, Y.-C. Wang, and J. Zheng, *J. Cosmol. Astropart. Phys.* 01 (2021) 042.
[16] M. Baryakhtar, A. Berlin, H. Liu, and N. Weiner, *J. High Energy Phys.* **06** (2022) 047.
[17] N. Song, S. Nagorny, and A. C. Vincent, *Phys. Rev. D* **104**, 103032 (2021).
[18] G. Aad *et al.* (ATLAS Collaboration), *J. High Energy Phys.* **07** (2021) 005.
[19] H.-J. He, Y.-C. Wang, and J. Zheng, *Phys. Rev. D* **104**, 115033 (2021).
[20] K. Harigaya, Y. Nakai, and M. Suzuki, *Phys. Lett. B* **809**, 135729 (2020).
[21] S. Jacobsen, K. Freese, C. Kelso, P. Sandick, and P. Stengel, *J. Cosmol. Astropart. Phys.* **10** (2021) 070.
[22] D. Borah, S. Mahapatra, D. Nanda, and N. Sahu, *Phys. Lett. B* **811**, 135933 (2020).
[23] W. Chao, Y. Gao, and M. j. Jin, arXiv:2006.16145.
[24] M. Dutta, S. Mahapatra, D. Borah, and N. Sahu, *Phys. Rev. D* **103**, 095018 (2021).
[25] W.-Y. Keung, D. Marfatia, and P.-Y. Tseng, *J. High Energy Astrophys.* **30**, 9 (2021).
[26] A. Aboubrahim, M. Klasen, and P. Nath, *J. High Energy Phys.* **02** (2021) 229.
[27] J. A. Dror, G. Elor, and R. McGehee, *Phys. Rev. Lett.* **124**, 18 (2020).
[28] J. A. Dror, G. Elor, and R. McGehee, *J. High Energy Phys.* **02** (2020) 134.

- [29] J. A. Dror, G. Elor, R. McGehee, and T.-T. Yu, *Phys. Rev. D* **103**, 035001 (2021).
- [30] Y. Kahn and T. Lin, *Rep. Prog. Phys.* **85**, 066901 (2022).
- [31] Z.-L. Liang, C. Mo, and P. Zhang, *Phys. Rev. D* **104**, 096001 (2021).
- [32] E. Andersson, A. Bökmark, R. Catena, T. Emken, H. K. Moberg, and E. Åstrand, *J. Cosmol. Astropart. Phys.* **05** (2020) 036.
- [33] P. W. Graham, D. E. Kaplan, S. Rajendran, and M. T. Walters, *Phys. Dark Universe* **1**, 32 (2012).
- [34] R. Essig, M. Fernandez-Serra, J. Mardon, A. Soto, T. Volansky, and T.-T. Yu, *J. High Energy Phys.* **05** (2016) 046.
- [35] I. Lazanu, M. L. Ciurea, and S. Lazanu, *Astropart. Phys.* **44**, 9 (2013).
- [36] R. Essig, A. Manalaysay, J. Mardon, P. Sorensen, and T. Volansky, *Phys. Rev. Lett.* **109**, 021301 (2012).
- [37] R. Essig, J. Mardon, and T. Volansky, *Phys. Rev. D* **85**, 076007 (2012).
- [38] B. Lehnert, H. Ramani, M. Hult, G. Lutter, M. Pospelov, S. Rajendran, and K. Zuber, *Phys. Rev. Lett.* **124**, 181802 (2020).
- [39] R. Essig, J. Pradler, M. Sholapurkar, and T.-T. Yu, *Phys. Rev. Lett.* **124**, 021801 (2020).
- [40] S. Knapen, J. Kozaczuk, and T. Lin, *Phys. Rev. Lett.* **127**, 081805 (2021).
- [41] M. Ibe, W. Nakano, Y. Shoji, and K. Suzuki, *J. High Energy Phys.* **03** (2018) 194.
- [42] D. Baxter, Y. Kahn, and G. Krnjaic, *Phys. Rev. D* **101**, 076014 (2020).
- [43] N. F. Bell, J. B. Dent, B. Dutta, S. Ghosh, J. Kumar, and J. L. Newstead, *Phys. Rev. D* **104**, 076013 (2021).
- [44] G. Grilli di Cortona, A. Messina, and S. Piacentini, *J. High Energy Phys.* **11** (2020) 034.
- [45] Y. Hochberg, E. D. Kramer, N. Kurinsky, and B. V. Lehmann, *Phys. Rev. D* **107**, 076015 (2023).
- [46] J. Smirnov and J. F. Beacom, *Phys. Rev. Lett.* **125**, 131301 (2020).
- [47] U. K. Dey, T. N. Maity, and T. S. Ray, *J. Cosmol. Astropart. Phys.* **03** (2017) 045.
- [48] U. K. Dey, T. N. Maity, and T. S. Ray, *Phys. Rev. D* **99**, 095025 (2019).
- [49] T. N. Maity and T. S. Ray, *J. Cosmol. Astropart. Phys.* **11** (2019) 033.
- [50] E. Kuflik, M. Perelstein, N. R.-L. Lorier, and Y.-D. Tsai, *Phys. Rev. Lett.* **116**, 221302 (2016).
- [51] Y. Hochberg, E. Kuflik, T. Volansky, and J. G. Wacker, *Phys. Rev. Lett.* **113**, 171301 (2014).
- [52] Y. Hochberg, E. Kuflik, H. Murayama, T. Volansky, and J. G. Wacker, *Phys. Rev. Lett.* **115**, 021301 (2015).
- [53] J. M. Cline, H. Liu, T. Slatyer, and W. Xue, *Phys. Rev. D* **96**, 083521 (2017).
- [54] C. F. Bunge, J. A. Barrientos, and A. V. Bunge, *At. Data Nucl. Data Tables* **53**, 113 (1993).
- [55] D. S. Akerib *et al.* (LUX Collaboration), *Phys. Rev. Lett.* **118**, 021303 (2017).
- [56] X. Cui *et al.* (PandaX-II Collaboration), *Phys. Rev. Lett.* **119**, 181302 (2017).
- [57] E. Aprile *et al.* (XENON Collaboration), *Phys. Rev. Lett.* **121**, 111302 (2018).
- [58] D. S. Akerib *et al.* (LUX Collaboration), *Phys. Rev. D* **93**, 072009 (2016).
- [59] E. Aprile *et al.* (XENON Collaboration), *Phys. Rev. D* **102**, 072004 (2020).
- [60] B. Yan *et al.* (PandaX-II Collaboration), *Chin. Phys. C* **45**, 075001 (2021).
- [61] J. F. Navarro, C. S. Frenk, and S. D. M. White, *Astrophys. J.* **490**, 493 (1997).
- [62] Q.-H. Cao, R. Ding, and Q.-F. Xiang, *Chin. Phys. C* **45**, 045002 (2021).
- [63] J. Kopp, V. Niuro, T. Schwetz, and J. Zupan, *Phys. Rev. D* **80**, 083502 (2009).
- [64] E. Aprile *et al.* (XENON Collaboration), *Phys. Rev. Lett.* **129**, 161805 (2022).
- [65] P. Agnes *et al.* (DarkSide Collaboration), *Phys. Rev. Lett.* **121**, 111303 (2018).
- [66] M. Cirelli, N. Fornengo, and A. Strumia, *Nucl. Phys.* **B753**, 178 (2006).
- [67] L. Lopez Honorez, E. Nezri, J. F. Oliver, and M. H. G. Tytgat, *J. Cosmol. Astropart. Phys.* **02** (2007) 028.
- [68] K. Petraki, M. Postma, and M. Wiechers, *J. High Energy Phys.* **06** (2015) 128.
- [69] K. Petraki, M. Postma, and J. de Vries, *J. High Energy Phys.* **04** (2017) 077.
- [70] D. J. Fixsen, E. S. Cheng, J. M. Gales, J. C. Mather, R. A. Shafer, and E. L. Wright, *Astrophys. J.* **473**, 576 (1996).
- [71] P. Arias, D. Cadamuro, M. Goodsell, J. Jaeckel, J. Redondo, and A. Ringwald, *J. Cosmol. Astropart. Phys.* **06** (2012) 013.
- [72] S. D. McDermott and S. J. Witte, *Phys. Rev. D* **101**, 063030 (2020).
- [73] S. J. Witte, S. Rosauero-Alcaraz, S. D. McDermott, and V. Poulin, *J. High Energy Phys.* **06** (2020) 132.
- [74] A. Caputo, H. Liu, S. Mishra-Sharma, and J. T. Ruderman, *Phys. Rev. Lett.* **125**, 221303 (2020).
- [75] A. Caputo, H. Liu, S. Mishra-Sharma, and J. T. Ruderman, *Phys. Rev. D* **102**, 103533 (2020).
- [76] I. M. Bloch, R. Essig, K. Tobioka, T. Volansky, and T.-T. Yu, *J. High Energy Phys.* **06** (2017) 087.
- [77] G. Alonso-Álvarez, F. Ertas, J. Jaeckel, F. Kahlhoefer, and L. J. Thormaehlen, *J. Cosmol. Astropart. Phys.* **11** (2020) 029.
- [78] H. An, M. Pospelov, J. Pradler, and A. Ritz, *Phys. Rev. D* **102**, 115022 (2020).
- [79] L. H. Nguyen, A. Lobanov, and D. Horns, *J. Cosmol. Astropart. Phys.* **10** (2019) 014.
- [80] M. J. Stott, *arXiv:2009.07206*.
- [81] A. Caputo, A. J. Millar, C. A. J. O'Hare, and E. Vitagliano, *Phys. Rev. D* **104**, 095029 (2021).
- [82] G. F. Giudice, D. Kim, J.-C. Park, and S. Shin, *Phys. Lett. B* **780**, 543 (2018).
- [83] K. Agashe, Y. Cui, L. Necib, and J. Thaler, *J. Cosmol. Astropart. Phys.* **10** (2014) 062.
- [84] J. D. Lewin and P. F. Smith, *Astropart. Phys.* **6**, 87 (1996).
- [85] C. Amole *et al.* (PICO Collaboration), *Phys. Rev. Lett.* **118**, 251301 (2017).